Biosensors and Bioelectronics 131 (2019) 104–112

Contents lists available at ScienceDirect

Biosensors and Bioelectronics

journal homepage: www.elsevier.com/locate/bios

In situ cancer diagnosis through online plasmonics

Médéric Loyez[a,*], Jean-Charles Larrieu[b], Samia Chevineau[a], Myriam Remmelink[c], Dimitri Leduc[d], Benjamin Bondue[d], Pierre Lambert[b], Jacques Devière[e], Ruddy Wattiez[a], Christophe Caucheteur[f]

[a] Proteomics and Microbiology Department, University of Mons, 6 Av. du Champ de Mars, 7000 Mons, Belgium
[b] TIPs Department (CP 165/67), Université libre de Bruxelles, Av. F.D. Roosevelt, 50 B,1050 Brussels, Belgium
[c] Department of Pathology, Université Libre de Bruxelles, Hôpital Erasme, 808 Route de Lennik, 1070 Brussels, Belgium
[d] Chest Department, Université Libre de Bruxelles, Hôpital Erasme, 808 Route de Lennik, 1070 Brussels, Belgium
[e] Laboratory of Experimental Gastroenterology, Université Libre de Bruxelles, Hôpital Erasme, 808 Route de Lennik, 1070 Brussels, Belgium
[f] Electromagnetism and Telecommunication Department, University of Mons, 31 Bld Dolez, 7000 Mons, Belgium

ARTICLE INFO

Keywords:
Optical fiber
Surface plasmon resonance
Biomarker
Cancer
Catheter
Endoscopy
Biosensing

ABSTRACT

Most cancer diagnoses rely on biomarkers detection. This could be improved if directly conducted in suspicious cancer spots, preventing the need for biopsy. Lung cancer remains a perfect study-case for such a development, as it is generally detected at advanced stage and is in the need for early diagnosis techniques. To this aim, we have designed a minimally invasive catheter-embedded biosensor. It combines a specific grating structure photo-imprinted in a telecommunication-grade optical fiber and an overlay made of a thin metal coating on which receptors are grafted, yielding plasmonic coupling. Our optrode targets a type of cytokeratins, overexpressed at the surface of cancer cells. It was assayed *ex vivo* in resected lung tissues collected from a dozen of patients. Biosensing responses were confirmed by immunohistochemistry, conducted on the same samples. In addition to accurate biosensing, our gratings inherently enable force-sensing features, which also allow a fine positioning of the probe in the tissue. Finally, the *in vivo* navigation of the bronchoscope-embedded sensor was validated into pig lungs. These achievements are a critical milestone towards the development of this micro/nano biosensor as a cost-effective and weakly invasive diagnostic tool for applications in areas of critical access such as brain, liver or prostate.

1. Introduction

Cancer is among the leading cause of death worldwide. Global mortality rates related to cancer has been decreasing for years in developed countries, especially because of diagnosis and therapies improvements, in addition to preventive interventions. However, lung, liver, stomach or pancreas cancers lag behind and remain difficult to target in first stages. Early cancer diagnosis is thus a key factor to face with the spiraling number of new cases and with high costs of care (Cronin et al., 2018).

Our study is part of this ambitious field of research and is based on lung cancer, which is the leading cause of death from cancer (Wong et al., 2017; Hirsch et al., 2016). This is largely due to the late diagnosis of the disease. Its mortality rate reaches 80–85% within 5 years after diagnosis, when it can decrease down to 45% if the disease is detected at an earlier stage, ensuring better patient care (Malvezzi et al., 2017). These findings stress the need for the development of new diagnostic tools on the ropes on precocious lung cancer detection.

Numerous and reliable techniques are commonly used in medical field to evaluate the severity of the cancer and its staging: imaging, bronchoscopy, mediastinoscopy, among others (Van der Aalst et al., 2016). The need for new diagnostic tools is highly required in practice to achieve minimally-invasive approaches and to ensure immediate tissue analysis, since most of the routine methods currently require biopsies (Maldonado and Jett, 2013).

Among the most innovative techniques related to cancer detection, *in situ* Raman spectroscopy (Huang et al., 2003; Salehi et al., 2014) and real-time imaging (Li et al., 2015) provide a panel of molecular detections and are able to discriminate healthy tissues from tumoral ones. They are really expected to guide the surgery and avoid remains of cancerous spots after tumor resection (Karabeber et al., 2014).

Regarding the diagnostic methods currently under development, major advances were recently reported in biological analysis through *e.g.* patient sputum tests (Hubers et al., 2013), artificial noses (Adiguzel and Kulah, 2015) or eNoses (Hubers et al., 2014), circulating tumor cells (CTCs) detection in blood samples (O'Flaherty et al., 2012; Ilie

* Corresponding author.
E-mail address: mederic.loyez@umons.ac.be (M. Loyez).

https://doi.org/10.1016/j.bios.2019.01.062
Received 3 December 2018; Received in revised form 23 January 2019; Accepted 27 January 2019
Available online 18 February 2019
0956-5663/

et al., 2014), microRNA (Zaporozhchenko et al., 2018) or exosomal proteins as novel potential biomarkers for lung cancer (Sandfeld-Paulsen et al., 2016). The actual trends in biosensors developments are also shifting towards less invasive and remote monitoring systems, to simplify their use and provide user-friendly interfaces. Multiplexing is also a key factor to enhance the precision of the analysis. Although cutting edge cancer biosensors are under development, they are still far from clinical rationale, and commercial setups are still in their infancy (Sankara Aditya Jayanthi et al., 2017).

Current lung cancer diagnosis techniques mostly rely on microscopic sections analysis or *in vitro* immunoassays aiming at biomarker detection. Some of the most commonly tracked biomarkers are the thyroid transcription factor (TTF-1) (Huang et al., 2017), the epidermal growth factor (EGFR) (Sharma et al., 2007), Kirsten rat sarcoma (KRAS) (Santis et al., 2011), the anaplastic lymphoma kinase (ALK) (Gridelli et al., 2015), or the carcinoembryonic antigen (CEA) (X et al., 2012), which are used in routine in clinical practice. Their combined revelation is often needed to ensure and validate the diagnosis through the identification of the cancer type. Recent studies have also pointed out new molecules to distinguish lung cancer subtypes, such as beta-arrestin-1 (El-Khoury et al., 2018) or SPATS2 (Takamochi et al., 2016), among a large number of other markers. Many of them were discovered through new “omics”-based technologies and are of interest for diagnosis, prognosis and/or response to treatments while detected with *in vitro* assays. This is particularly true with the development of personalized cancer therapy (Vargas and Harris, 2016; Barlesi et al., 2016; O’Byrne et al., 2011).

Another way of approaching lung cancer diagnosis is to bring a biosensor directly into contact with a suspicious tissue and therefore avoid the need for any sample collection. To this aim, our approach involves telecommunication-grade single-mode optical fibers, which are flexible and reliable waveguides inherently suited to be inserted into catheters and/or endoscopes (Short et al., 2008). Combined to their miniaturized size and easy light injection, a valuable asset is their ability to passively and remotely bring information from the distal end to the monitoring system.

Optical fiber sensors are of interest for a large number of diseases and cancers, especially when they are hard to reach, such as for thyroid and brain cancers. They could avoid the need for liquid punctures as they can be directly inserted in a needle and adapted for a large range of molecules (Guo et al., 2017). Detection of various targets in various types of body fluids such as blood (Lu et al., 2017), urine (Guo et al., 2016) and saliva (Usha et al., 2017) were recently reported.

Different optical fiber configurations can be exploited, all based on the local exposition of the core-guided light to the surrounding medium. This is usually obtained by bending the fiber or by removing the cladding totally or partially, through mechanical polishing or chemical etching (Caucheteur et al., 2015). An alternative approach consists in photo-imprinting periodic structures in the fiber core, such as long period fiber gratings (LPFGs) (Bandyopadhyay et al., 2017; Pilla et al., 2011) or tilted fiber Bragg gratings (TFBGs) (Chiavaioli et al., 2017; Albert et al., 2012). All these configurations are able to excite surface plasmon polaritons when they are surrounded by a thin noble metal and illuminated with appropriately polarized light (Barnes et al., 2003). The surface plasmon resonance (SPR) can be tracked in their corresponding spectrum, to obtain surface (bio)chemical sensing enhancements compared to bare configurations (Antohe et al., 2016; Loyez et al., 2018). Hence, SPR-based optical fiber sensors are a miniaturized counterpart to the Kretschmann prism configuration used in commercial devices, offering easy operation with small amounts of analytes (Gopinath, 2010; Homola et al., 1999).

The underpinnings of our work rely on original SPR-based optical fibers structures, namely gold-coated TFBGs (Ribaut et al., 2016). Their tilted refractive index modulation couples near IR-light from the core to the cladding into tens of narrowband mode resonances, yielding refractive index-sensitive evanescent waves in the surrounding medium, while preserving the optical fiber integrity (Shevchenko and Albert, 2007). Core mode coupling at the Bragg wavelength is also provided, which is used in the following for force sensing. In addition, the implemented tilted refractive index modulation breaks the cylindrical symmetry of the fiber core, yielding birefringence and therefore inducing differential couplings between radially- and azimuthally-polarized high-order cladding modes. Radially-polarized mode resonances are the only ones able to excite surface plasmon waves, offering highly valuable sensing possibilities (Caucheteur et al., 2011). Gold-coated TFBGs with immobilized cytokeratin-17 antibodies are used in this paper to detect cancer cell surface biomarkers (Cytokeratin-17 proteins) reflecting the presence of lung tumor cells. By the way, this sensing method can also be implemented with numerous types of other receptors such as aptamers (Shevchenko et al., 2011), DNA (Pollet et al., 2009) or enzymes (Jiang et al., 2018) targeting molecules of very different nature.

We focus here on a relevant clinical issue: immediate lung cancer diagnosis in the distal bronchial tree. To this aim, we have manufactured a packaged optrode comprising a specifically-designed catheter and functionalized gold-coated TFBGs. It was intensively used to perform *in situ* measurements in fresh human lung lobectomies as well as in living pig. It combines the expertise of multidisciplinary fields including biophotonics, plasmonics, bioengineering and endoscopy.

Our work tightly exploits the dual nature of the coupling provided by TFBGs. Indeed, besides the biological detection provided by the cladding mode resonances spectrum of our gratings, we demonstrate that the core mode also provides relevant information about the penetration force, which can be used to discriminate healthy from abnormal tissue and therefore correctly position the optrode in the area of interest. Hence, our architecture provides two sensing modalities, combining biological and biomechanical information in a single optical fiber.

In this paper, we first present the design and optimization of this biosensing strategy. We then demonstrate its clinical relevance and show its performances, obtained from experiments conducted *ex vivo* in resected human lung tissues and *in vivo* in anesthetized pig.

2. Material and methods

2.1. Design and fabrication process of the endoscopic catheter

The catheter is designed to obtain enough flexural rigidity but also enough axial stiffness for the catheter not to kink, making the navigation impossible. The catheter is realized in Polyoxymethylene (POM) Hostaform C2521 Natural (E = 2.6 GPa) by extrusion to allow these features. The catheter dimensions are ϕ_{inner} = 1.2 mm ± 0.05 mm, ϕ_{outer} = 1.6 mm ± 0.05 mm, L = 2 m. The distal conformation of the tip is obtained by thermo-moulding with semi-automatic machinery. An electrical current is applied inside a mould which wall thickness is greatly decreased at a specific location, where heat is thus concentrated *via* Joules heating. The extruded tube is then put inside the mould, heated, and then pushed. The window is manually patterned on the side by cutting a 4 mm long area with a jig under microscope.

The proximal crimping collar is a cylindrical bock of 1 mm in height and 1.2 mm in diameter with two passing holes in its core, both of 0.25 mm in diameter allowing the insertion of SMF-28 optical fibers with a corresponding diameter of 250 µm. The distal crimping collar has two passing slots of 0.13 mm in thickness that are patterned along its height to immobilize the fibers in the tip of the catheter.

Crimping collars are fixed inside the catheter using medical-grade glue. The packaging is then inserted in the bronchoscope, where navigation is performed with a rigid or flexible extension connected to CCD camera. The complete characterization of the flexural rigidity of the catheter is presented in Table 1.

The flexural rigidity of a rigid body (EI) characterizes its ability to resist to bending. It consists in the product between the Young's Modulus of the considered rigid body and the moment of inertia of the

Table 1
Values of flexural rigidity (EI [N m^2]) for the manufactured POM catheter.

Catheter	E (MPa)	I (m^4)	EI (Nm^2)
POM catheter φ_{outer} = 1.1 mm	1.860	0.040×10^{-12}	74×10^{-6}
Catheter	1.860	0.220×10^{-12}	409×10^{-6}
POM catheter φ_{outer} = 2.1 mm	1.860	0.545×10^{-12}	1.014×10^{-6}

structure (I), and therefore takes into account the intrinsic properties of the material via E and the geometry of the rigid body with (I).

2.2. Tilted fiber Bragg gratings manufacturing

Standard telecommunication-grade optical fibers (SMF-28, Ø250 µm single-mode silica OF, Corning) were used to connect each sensor. Photosensitive optical fibers (PS-1250) were used with the NORIA system (NorthLab Photonics) to inscribe permanent refractive index modulations in the fiber core (Ø 8 µm) to obtain 7° tilted fiber gratings (Coherent Excistar XS 500 Hz at 193 nm). The gratings were produced through a uniform phase-mask (1090 nm period) tilted in the plane perpendicular to the incident laser beam.

2.3. SPR-TFBGs functionalization

A gold deposition of 50 nm was performed by sputter-coater under vacuum and a thermal annealing at 200 °C was applied during two hours to increase the adhesion of the gold film on the silica surface. SPR-TFBGs were then cleaned with absolute ethanol and functionalized with anti-CK17 antibodies. First, a SAM of alkanethiols was immobilized on the gold film (S_2PEG_6COOH 2 mM in ethanol during 16 h). Then, OFs were immersed in NHS (N-hydroxysuccinimide 0.1 M)/EDC (N-(3-Dimethylaminopropyl)-N′-Ethylcarbodiimide Hydrochloride 0.5 M) in pure water during 20 min. After that, fibers were immersed into anti-CK17 antibodies solution (20 µg/mL in PBS buffer) during 1 h30. They were finally rinsed and blocked with BSA 5% (w/v) in PBS during 1 h30, dried, and stored in dry conditions.

2.4. Optical fibers interrogation

A reflective mirror is added at the cleaved end of the grating to ensure reflection and the optical fiber grating is connected to the MicronOptics interrogator (National Instruments), through a light polarizer. Near-infrared spectra are then recorded using an automatic saving software in-house developed with a LabView 7.0 program. A demodulation is also performed after data acquisition using a MATLAB script, to select and analyze the spectral mode of interest.

2.5. Human lobectomy analysis

Human samples, directly analyzed after their collection, were prepared by doctors for the test. They were placed on an experimental table where the device, placed on a carriage, was brought near the lobectomy. The sensor was then placed on a fixed static holder and the lobectomy was brought into contact using a one-axis automated lift. The force sensing was performed both with the optical interrogator and with a scale placed under the tissue. The biosensing was performed in both healthy and tumoral tissue during 5 min after insertion. The healthy tissue was considered as the reference signal while its evolution was captured each 30 s during measurements.

2.6. Immunohistochemistry protocol

Sections were collected from the same tissues analyzed with the optical fiber gratings. The sections were stained with Mayer's Hemalum, marking the nuclei of cells in purple/blue. The Cytokeratin-17 proteins were marked thanks to anti-CK17 antibodies and reaction with DAB molecules provoking the apparition of brown precipitates at the protein location sites. Finally, a luxol-blue staining was applied to slightly color all the structures non-stained by the two previously mentioned colorations. Detailed protocol of Cytokeratin 17 staining using immunohistochemistry is decribed in Supplementary information.

2.7. Immunohistochemistry analysis

Immunohistological sections were scanned using an automated system (Hamamatsu Nanozoomer) and observed through NDP View interface. The CK17 quantification was performed on squamous cell carcinoma, adenorcarcinoma and neuroendocrine cases that were previously analyzed by the optical fiber approach on the freshly collected tissue. The quantification was performed through computer analysis. A mean ± sd for both types of cancer was calculated as the % of marked areas on the sections.

3. Results

3.1. Design of the endoscope embedded fiber optic sensor

The sensing architecture developed and used in this work is an optrode made of a gold-coated TFBG followed by a gold mirror deposited on the cleaved fiber end face (Fig. 1**a**). The typical reflected amplitude spectrum of this configuration immersed into liquid solutions or soft matter is displayed in (Fig. 1**b**). This spectrum is recorded using P-polarized input lightwaves, so that the electric field of the evanescent wave is radial to the gold interface and can tunnel inside. In this case, SPR excitation is achieved for cladding mode resonances with an effective refractive index that matches the one of the surrounding medium. This is spectrally characterized by an attenuation of those cladding mode resonances, whose amplitude is modulated by the SPR envelope. The SPR area is highly sensitive to surface refractive index variations, enabling its monitoring for biosensing. Another important feature of the spectrum is the core mode resonance appearing at the Bragg wavelength. The latter corresponds to light remaining confined in the fiber core and is therefore not sensitive to surrounding refractive index changes. However, it is very sensitive to mechanical stress. Hence, it is monitored during our experiments to evaluate the penetration force applied on the fiber tip during the insertion of the packaging into the analyzed sample. These two combined sensing modalities make our sensing architecture particularly relevant for the target application.

We designed and developed a unique catheter aiming at housing our optical fiber sensor while allowing its access in different areas of lungs, from the apex to the base (Fig. 1**c**). Its structure, manufactured by extrusion of a biocompatible polymer has been selected to prevent any decrease of bending abilities while ensuring the preservation of the optical fiber integrity and its good operation.

For assembly, the optical fiber sensor is pulled through the catheter tube and then fixed in position thanks to two distal crimping collars. These ones are also strongly fixed to the packaging thanks to medical-grade glue (Fig. 1**d**).

The crimping collars are patterned to enable robust anchoring of the optical fibers at the tip of the needle where an aperture of 4 mm has been laser cut. This aperture brings the sensor into contact with the sample and plays a major role in the interaction between biofluids and sensing areas of TFBGs. The inner diameter of 1.2 mm of the packaging tube can also be involved in the aspiration of biofluids by capillary effect and be used as internal self-powered microfluidic channel, which could be further studied to perform *in situ* punctures (Fig. 1**e**).

Beyond the biosensor implementation, the catheter has been conceived to be universally inserted into different types of bronchoscopes (Fig. 1**f**). The bronchoscope considered as reference for the design process is the commonly used Olympus BF-1T180, with a working

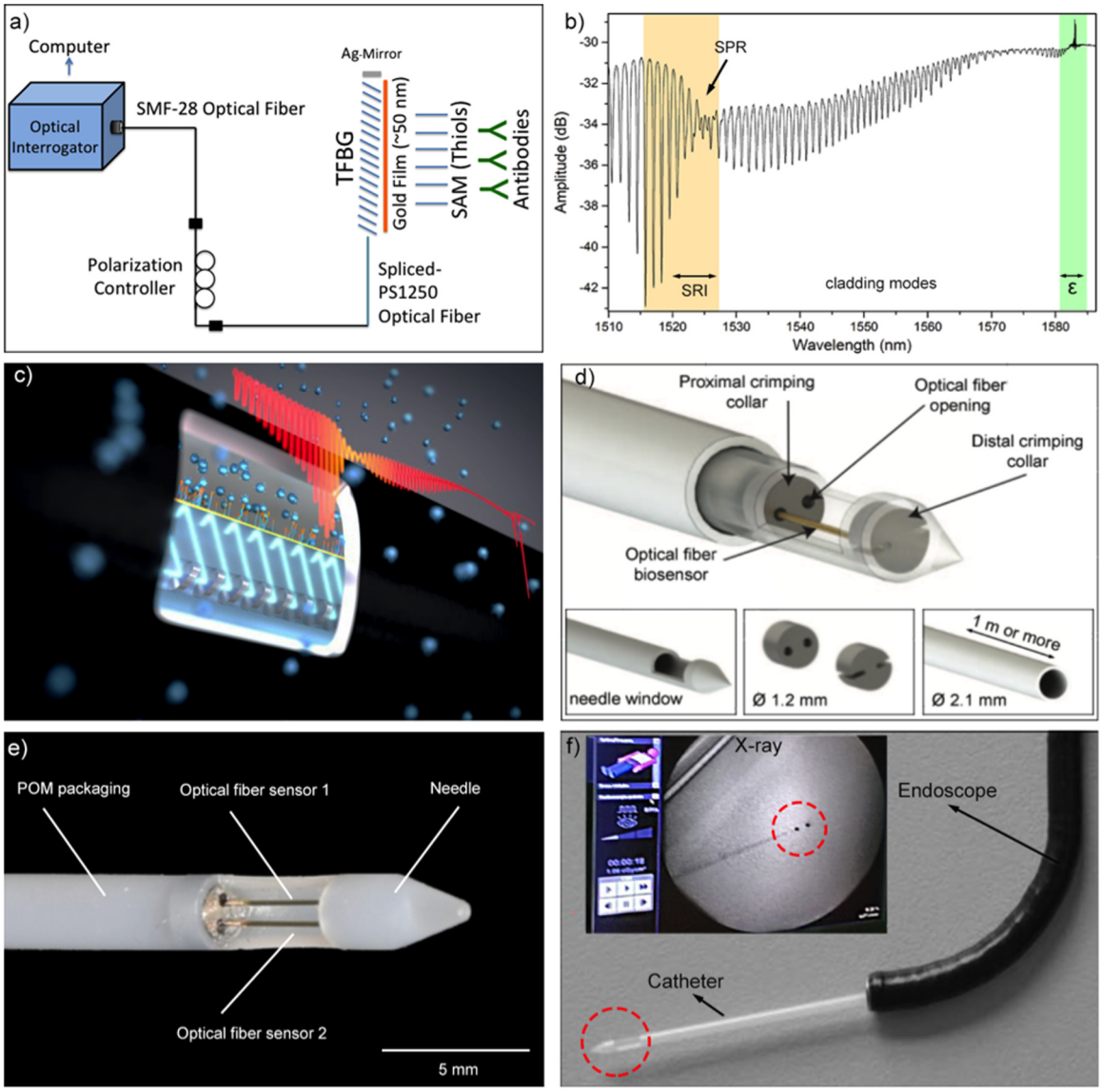

Fig. 1. (a) Scheme of the portable experimental setup used for the TFBG interrogation. (b) The spectrum of gold-coated TFBG sensor yields SPR excitation ensuring biodetection of molecular target (in yellow) when the Bragg wavelength (in green) brings biomechanical information. (c) Artistic view of the embedded optical fiber sensor with the opened sensing window. (d) 3D representation of parts of the packaging. (e) Picture of the assembled optrode with two embedded gold-coated TFBGs. (f) The catheter can be easily inserted into endoscopes, ensuring sufficient maneuverability and bending rates. The crimping collars made of stainless steel also ensure its monitoring in real time under X-rays.

channel of 3 mm. To ensure compatibility with other tools equipped with smaller working channels, the largest dimension of the optrode has been set to 2.2 mm. The developed prototype can host two optical fibers (for instance to simultaneously target two biomarkers) but dimensions could allow the insertion of 5 different optical fiber sensors.

The decreasing size of bronchi makes the navigation through the lungs difficult and constitutes an important constraint in the design of bronchoscopic tools. Our device allows reaching the fifth generation of bronchi, making possible the exploration of thin cancer spots and peripheral lesions. To increase the precision of the intervention in these critical regions, inner crimping collars have been made in stainless steel, visible through fluoroscopy. This allows online monitoring of the catheter location, refining the positioning of the sensor extremity.

The distal end of the catheter has a conical form, ensuring a penetration of a few millimeters in a tissue. This thin insertion maintains the catheter in a fixed position during data acquisition and it was designed to be minimally harmful for the tissue.

3.2. Fiber optic detection of CK17 proteins in human tissues

Our experiments were conducted on freshly collected human lung lobectomies, which were firstly analyzed by doctors for TNM staging, and were then accessible for our research. The embedded optrodes were tested in tissues during 5 min in both healthy and tumoral parts, allowing sufficient data acquisition for biosensing. (Fig. 2**a**)

Deposited on a 1-axis automated lifting platform ensuring constant and identical insertion speed of the immobilized sensor, the samples were first tested in healthy parts considered as the reference signaling, where no detection (or low-level detection) occurred. After that, the optrodes were immersed in tumoral parts showing located spectral deviation due to the CK17-protein interaction with the fiber surface, according to its overexpression in cancers.

Optical fiber sensors functionalized with anti-CK17 antibodies show no significant response within 5 min in healthy part of lobectomy, as data show for a detection experiment on (Fig. 2**b).**

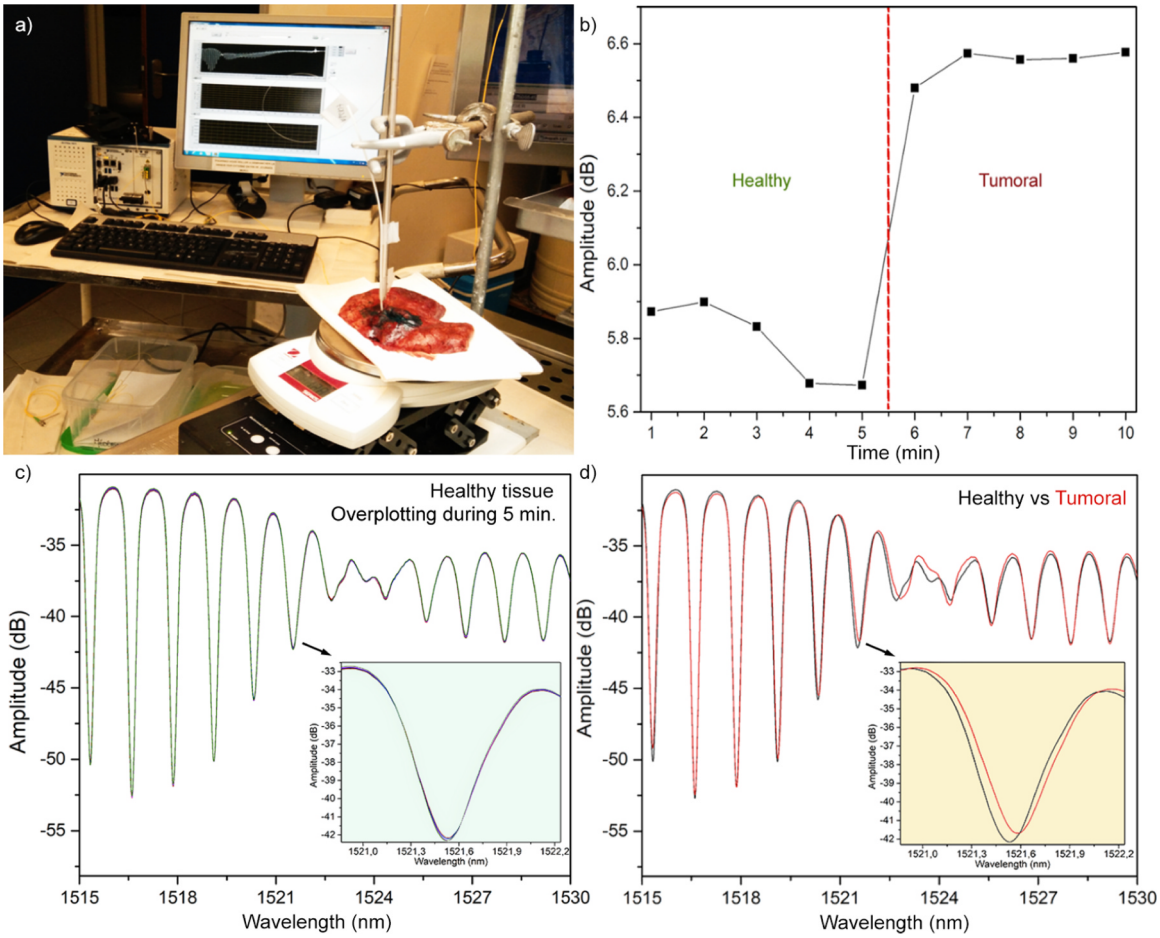

Fig. 2. (a) Picture of the experimental set-up showing the insertion of the packaging into human lung tissue. (b) Peak-to-peak analysis for the detection of CK17 in both healthy and tumoral tissues as a function of time. (c) Over-plotted spectra from 1 to 5 min in healthy tissue. (d) Over-plotted spectra after 5 min in healthy tissue in black *vs.* tumoral tissue in red. (For interpretation of the references to color in this figure legend, the reader is referred to the web version of this article.)

However, after its insertion into the tumorous part, the behavior of the spectral sensitive area progressively changes. It evolves as function of time, but quickly shows a significant response greater than 0.5 dB, experimentally fixed as our detection threshold. The biological response highly depends on the protein concentration and availability for interaction with the optrode. However, the expression of this protein is high enough to detect the presence of cancer cells within 1 min with this technique.

Tumors also remain very disparate and inhomogeneous, especially regarding the interaction area with the fiber tip, highly dependent on the location of the sensor in the tissue. Although this may hinder the detection, the reproducibility is not affected. The surface expression of the selected biomarker allows the sensor to only enter in contact with the tumor margins. It is also abundant into tumor masses and allows rapid detection in most of the cancerous spots analyzed.

Our SPR sensors are used in complex media. Therefore, reference measurements are of major importance (Fig. 2**c**). To ensure a stable acquisition, data were collected during 5 min in healthy areas and over-plotted to evaluate the few interactions occurring in this last.

To compensate any influence of temperature variation inside the tissue or external mechanical constraints during experiments, compensations of Bragg peak shifts and baseline variations were taken into account for all data analysis.

Once inserted in tumorous parts, strong interactions between cytokeratins-17 and antibodies immobilized on the sensor provoke intense variations of the surface-located refractive index, which impacts the modal behavior in the SPR region of TFBGs spectra, without effects on the other cladding (or core) mode resonances (Fig. 2**d**).

3.3. Penetration force measurements using native properties of TFBGs

TFBGs are inherently highly sensitive to mechanical constraints (Albert et al., 2012). Our prototype offers dual detection, combining biological response with fine penetration force measurements monitored through Bragg peak shifts. (Fig. 3**a**) The addition of a scale on the top of the automated platform, directly under the piece of tissue, allows us to directly verify the insertion force needed to penetrate the lobectomy, giving us supplementary biomechanical information about the experimental strength applied on the optrode. In our experimental conditions, the penetration force is mainly driven by the perforation of the pleura of the lobectomy. (Fig. 3**b**) However, interesting behaviors have been highlighted after the relaxation of that membrane, while the sensor reaches the targeted healthy or tumoral area.

In healthy parts, force measurements show similar profiles (Fig. 3**c**) while penetration forces in tumors reflect their structural heterogeneity. When most of tumors are denser than normal tissues due to the abundant proliferation of cells, highly advanced stages tumors also present necrotic regions leading to less important hardness in-between harder structures, and thus provoking lowered and fluctuating penetration forces patterns. (Fig. 3**d**)

Using these biomechanical features, it will be possible for the practicing surgeon to recognize the nature of the tissue and to obtain a numbered evaluation of the stiffness of that tissue, which is often left to the only feeling of the practitioner. It could be used as a verification method for the good positioning of the bronchoscopic optrode in the tumor, but also for the evaluation of its staging regarding the obtained penetration force behavior.

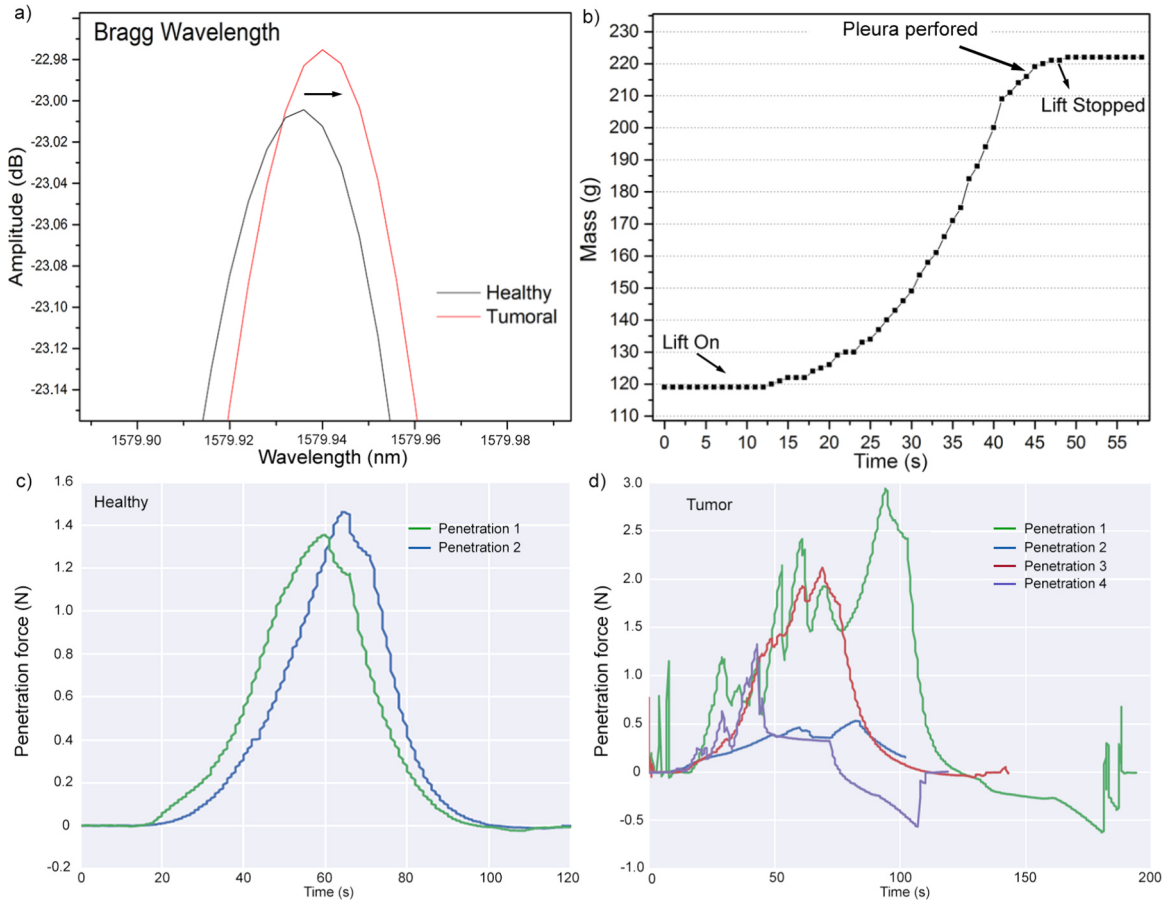

Fig. 3. (a) Bragg wavelength shifts of a gold-coated TFBG between healthy and tumoral tissues. (b) Penetration force slope measured with a scale placed under the lung lobetomy, where the catheter was inserted with a constant speed. (c) Penetration forces between healthy tissues and (d) tumorous tissues measured during the insertion of the packaged sensor at constant speed.

3.4. Validation of Cytokeratin-17 detection through immunohistochemistry

The previously described anti-CK17 probes were tested in lung tissues freshly resected from a dozen of patients. Results from these biosensing experiments are presented as a significant response between healthy and tumoral parts of each tissue, as a function of the analyzed cancer subtype. Negative controls using non-functionalized optical fiber gratings were also used, yielding sensing responses lower than 0.5 dB, experimentally considered as our detection threshold. This high sensing threshold ensures sufficient sensitivity while avoiding false positive detections, mainly due to noise effect into those complex samples. (Fig. 4**a**)

Immunohistochemistry has also been performed on the same analyzed tissues to assess the expression of CK17 in both healthy and tumoral samples. Histological sections cut from the previously analyzed patient's tissues were collected. These slices were cut in different angles to cover the 3D area examined with the optrode. The immunochemistry process (IHC) was performed using a 3,3'-diaminobenzidine marking (DAB) in order to color the sections in the visible range. The protocol used for this immunohistochemistry is presented in details in Supplementary information.

Thanks to this approach, we detected the presence of tumorous cells overexpressing the CK17 protein in squamous cell carcinoma, adenocarcinoma and neuroendrocrine cancers. Their expression-rate was calculated through the mean percentage of CK17-expressed areas, realized by image processing of 3 sections per case, of both healthy and tumoral tissues coming from the same patient. (Fig. 4**b**)

Healthy lung tissues have a very different structure from tumors in terms of cellular density. When healthy tissue sections are analyzed, the most present structures are alveoli, leading to low number of cells in a microscopic field. However, the tumoral parts present high cellular density, completely filling the gaps in between normal structures, and often presenting a dense extracellular matrix with fibrosis. Combining structure and density changes with levels of CK17 expression, the available quantity of biomarker proteins entering in contact with the optical fiber surface is higher in a dense tissue. However, the increased amount of cells does not lead to sufficient refractive index change at the interface between the optical fiber and the opened catheter window, which still allows sufficient specificity for molecular detection, as negative controls tested in these conditions do not show significant responses.

The CK17 protein is present in all the analyzed tumors (Fig. 4**c-e**) but with a higher expression rate in the neuroendocrine case analyzed, which also lead to a higher sensing response by our biosensor. Therefore, this experiment confirms the presence of the target and gives an approximated range of biomarker expression, which can be correlated with the biosensing response obtained with our probes. In some cases, we also observed high inflammation and fibrosis areas, which delimitate cancer cells as represented for a squamous cell cancer case, depicted in Fig. 4**c**. In non-squamous cell lung cancers (NSCLCs), we also noticed a higher level of expression of Cytokeratin-17 in the tumor margins, which is relevant for a minimally invasive catheter approach. Healthy tissue staining and negative-control IHC sections are presented in Supplementary information.

Experimental data obtained with optical fibers were correlated with traditionaly used diagnosis methods for the same analyzed tissues, and lead to a sensitivity of 80% and a specificity of 90.9%. This is largely due to the fine determination of the sensing threshold, achieved after

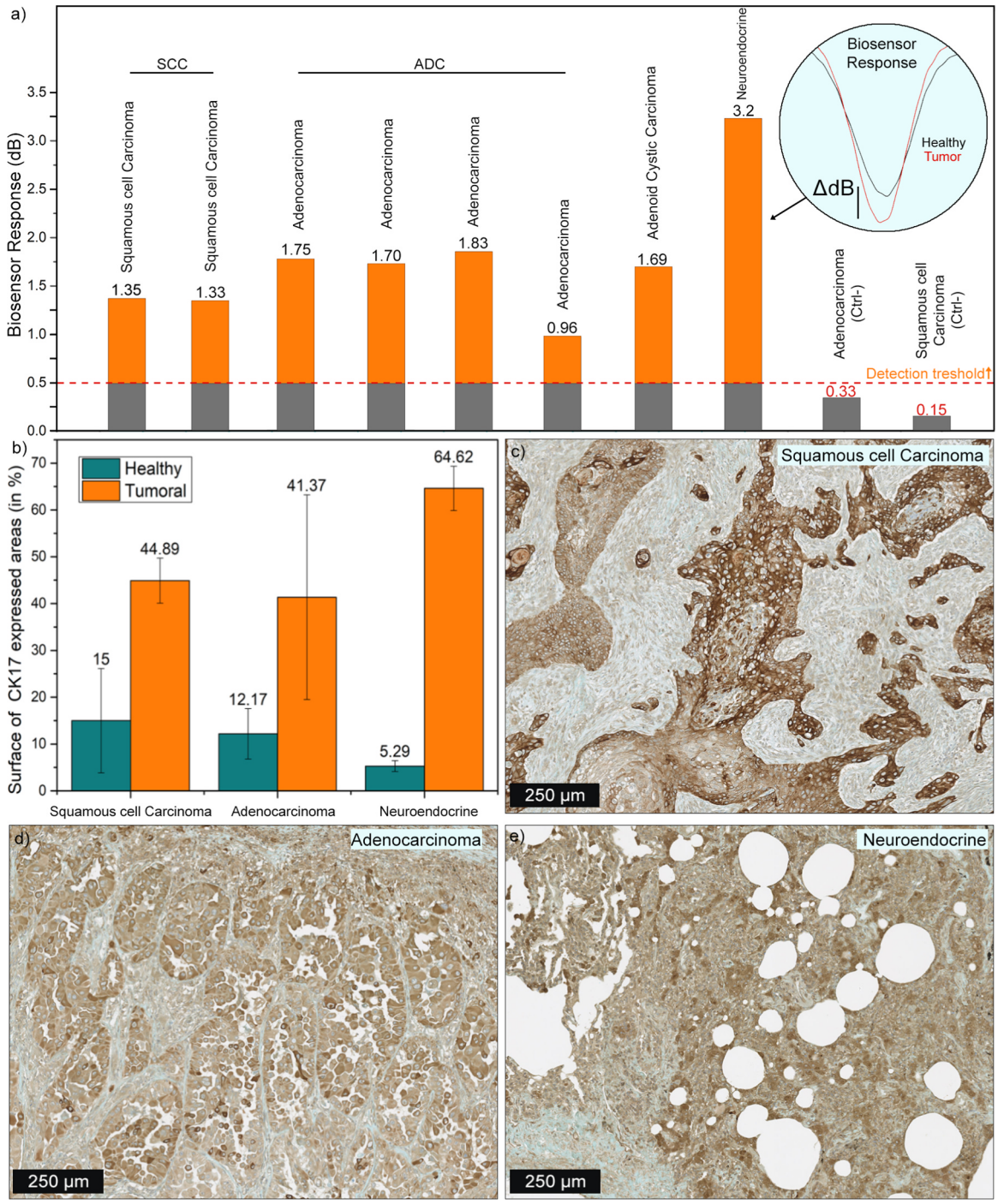

Fig. 4. (a) Histogram of the peak-to-peak analysis, showing the final biosensing response for the CK17 detection between healthy and tumoral areas of each tested tissue after 5 min. (b) Immunohistochemistry quantification of CK17-expressed areas on microscopic sections performed by image analysis. Staining of CK17 in human lung cancers previously analyzed with the optical sensors. Pictures of (c) Squamous Cell Carcinoma, (d) adenocarcinoma, (e) neuroendocrine.

numerous control tests in both healthy and tumoral environments, in addition to reliable surface blocking.

3.5. Endoscope navigation and SPR measurement into anesthetized pig

The navigation of the optrode inserted into a bronchoscope was tested in an anesthetized pig by an experimented pulmonologist. (Fig. 5**a**) The main aim of this experiment was to verify the easy operation of the device inside different areas of the lungs, while ensuring a stable SPR signal at the same time. The insertion of the bronchoscope into the respiratory tract and the location of the conic needle tip were monitored both with the optical view of the endoscope, connected to a CCD camera, and with fluoroscopy.

This first successful *in vivo* experiment strongly shows the possibility to use these SPR-TFBGs sensors for endoscopic analyses. The bronchoscope was able to reach upper regions of lungs which are the most difficult to reach. The monitoring of the sensor positioning by chest radiography allowed a fine control of the needle, thanks to the presence of crimping collars inside the conic end of the catheter. The maximum bending angle of the endoscope embedding the packaged optrode is close to the empty configuration of the endoscope itself, reaching ~124°. (Fig. 5**b**)

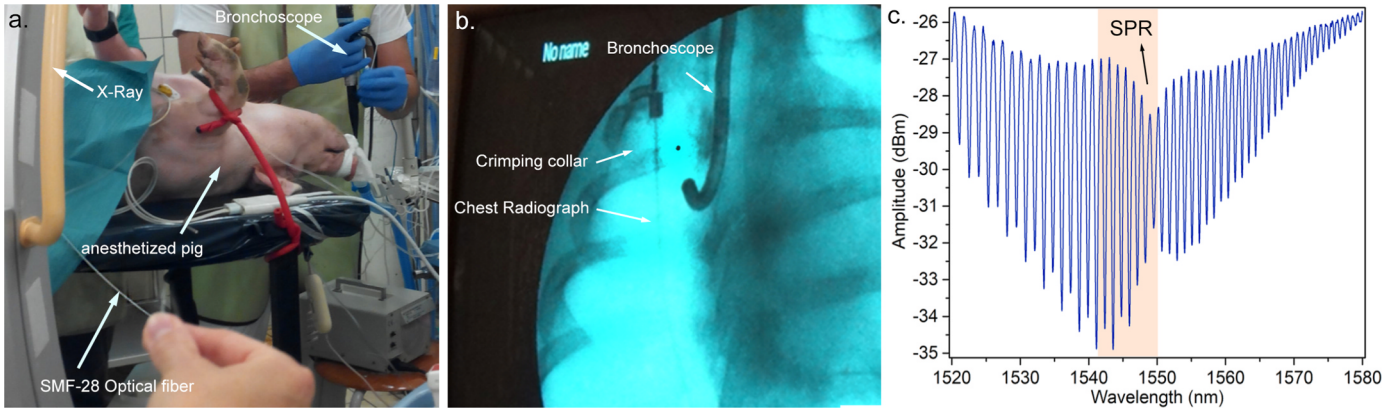

Fig. 5. (a) Picture of the anhestetized pig, with the live endoscope navigation performed by a surgeon from Erasme Hospital in Brussels, ULB. (b) Chest radiograph showing pig lungs and the endoscope, with the crimping collar indicating the location of the needle. (c) SPR signature obtained in pig lungs after insertion of the sensor in the upper lobe.

Finally, the SPR response presented was also obtained into the lungs, and was stable during 5 min of measurement, which correspond to the monitoring time also performed *ex vivo* on human lobectomy (Fig. 5**c**). These achievements are ensuring sufficient signal stability for further detection and open the way for potential *in vivo* catheteric detection.

4. Conclusion and prospects

Hard-to-reach cancers need novel perspectives of diagnosis to avoid invasive sampling and time wasting between assays, data acquisition and analysis. In that context, we propose a multidisciplinary approach combining biochemistry, photonics, engineering and endoscopy to develop a catheter embedded optical fiber sensor for *in situ* detection of lung cancer biomarkers. Experimental results show that our biocompatible endoscopic tool is able to navigate inside lungs with high flexibility. *Ex-vivo* assays performed on freshly resected human lobectomies from a dozen of patients show efficient detection of the target biomarker, allowing discrimination between healthy and cancerous tissues. The presence of the proteic target of interest, namely cytokeratin-17, was therefore validated through immunohistochemistry performed on the same analyzed samples. Using the inherent properties of TFBGs, the biological information was implemented with mechanical information providing an evaluation of the stiffness of the tissue, ensuring the good location of the sensor. Finally, the recent assessment of SPR signature into anesthetized pig lungs with sufficient stability and intensity opens the way for further *in vivo* experiments. Dual sensing and multi-target biodetection possibilities emerging from this minimally invasive and cost-effective prototype may be of interest in the medical community, fostering the future for online diagnostics of cancers.

Acknowledgements

We thank the Laboratory of Histology (University of Mons, Belgium), headed by Prof. Denis Nonclercq for the immunohistological staining and microscopic analysis. We also thank the DiaPath laboratory (CMMI Gosselies, Belgium) for the high quality automated scanning of the lung sections. We also warmly thank Dr. Clotilde Ribaut for her help and contribution to the experiments.

Funding sources

This research was funded by the European Research Council (ERC) through the starting independent researcher grant PROSPER (Grant Agreement no. 280161), by the F.R.S-FNRS (Associate Researcher Grant of C. Caucheteur), by the ARC research program of the UMONS-ULB academy (PREDICTION grant), and the Excellence of Science project (EOS ID 30467715), financially supported by Science Foundation-Flanders – FWO with project number G0F6218N. The research was also supported by the FRIA grant (F.R.S-FNRS) of M. Loyez.

Competing interests

The authors declare no conflicts of interests.

Credit author statement

- **Médéric Loyez,** data acquisition, analysis and writing.
- **Jean-Charles Larrieu,** design of the packaging, data acquisition and analysis.
- **Samia Chevineau,** validation of the target biomarker.
- **Myriam Remmelink, Dimitri Leduc and Benjamin Bondue,** access to samples and supervision.
- **Pierre Lambert,** supervision and data analysis.
- **Jacques Devière,** supervision at a medical level.
- **Ruddy Wattiez and Christophe Caucheteur,** conceptualization, surpervision, and data analysis.

Appendix A. Supporting information

Supplementary data associated with this article can be found in the online version at doi:10.1016/j.bios.2019.01.062.

References

Adiguzel, Y., Kulah, H., 2015. Biosens. Bioelectron. 65, 121–138.
Albert, J., et al., 2012. Laser Photon. Rev. 26, 1–26.
Antohe, I., et al., 2016. Sens. Actuators B. Chem. 229, 678–685.
Bandyopadhyay, S., et al., 2017. Appl. Opt. 56, 9846.
Barlesi, F., et al., 2016. Lancet 387, 1415–1426.
Barnes, W.L., et al., 2003. Nature 424, 824–830.
Caucheteur, C., et al., 2011. Appl. Phys. Lett. 99, 1–3.
Caucheteur, C., et al., 2015. Anal. Bioanal. Chem. 407, 3883–3897.
Chiavaioli, F., et al., 2017. Nanophotonics 6, 663–679.
Cronin, K.A., et al., 2018. Cancer 124, 2785–2800.
El-Khoury, V., et al., 2018. Br. J. Cancer.
Gopinath, S.C.B., 2010. Sens. Actuators B Chem. 150, 722–733.
Gridelli, C., et al., 2015. Nat. Rev. Dis. Prim. 21, 15009.
Guo, T., et al., 2016. Biosens. Bioelectron. 78, 221–228.
Guo, T., et al., 2017. Sensors 17, 1–20.
Hirsch, F.R., et al., 2016. Lancet 389, 299–311.
Homola, J., et al., 1999. Sens. Actuators B Chem. 54, 3–15.
Huang, T.W., et al., 2017. Sci. Rep. 7, 1–10.
Huang, Z., et al., 2003. Int. J. Cancer 107, 1047–1052.
Hubers, A.J., et al., 2013. Br. J. Cancer 109, 530–537.
Hubers, A.J., et al., 2014. J. Clin. Pathol. 67, 707–711.

Ilie, M., et al., 2014. PLoS One 9, 4–10.
Jiang, B., et al., 2018. Sens. Actuators B. Chem. 254, 1033–1039.
Karabeber, H., et al., 2014. ACS Nano 8, 9755–9766.
Li, T., et al., 2015. Sci. Rep. 5, 1–12.
Loyez, M., et al., 2018. Biosensors 8, 74.
Lu, J., et al., 2017. Anal. Chem. 89, 3664–3671.
Maldonado, F., Jett, J.R., 2013. Oncology 41, 17–27.
Malvezzi, M., et al., 2017. Ann. Oncol. 28, 1117–1123.
O'Byrne, K.J., et al., 2011. Lancet Oncol. 12, 795–805.
O'Flaherty, J.D., et al., 2012. Lung Cancer 76, 19–25.
Pilla, P., et al., 2011. Opt. Lett. 37, 4152–4154.
Pollet, J., et al., 2009. Biosens. Bioelectron. 25, 864–869.
Ribaut, C., et al., 2016. Biosens. Bioelectron. 77, 315–322.
Salehi, M., et al., 2014. Nanoscale 6, 2361–2367.
Sandfeld-Paulsen, B., et al., 2016. Mol. Oncol. 10.
Sankara Aditya Jayanthi, V.S.P.K., et al., 2017. Biosens. Bioelectron. 91, 15–23.
Santis, G., et al., 2011. PLoS One 6, e25191.
Sharma, S.V., et al., 2007. Nat. Rev. Cancer 7, 169–181.
Shevchenko, Y.Y., Albert, J., 2007. Opt. Lett. 32, 211–213.
Shevchenko, Y., et al., 2011. Anal. Chem. 83, 7027–7034.
Short, M. a., et al., 2008. Opt. Lett. 33, 711–713.
Takamochi, K., et al., 2016. BMC Cancer 16, 1–10.
Usha, S.P., et al., 2017. Biosens. Bioelectron. 87, 178–186.
Van der Aalst, C.M., et al., 2016. Lancet Respir. Med. 4, 749–761.
Vargas, A.J., Harris, C.C., 2016. Nat. Rev. Cancer 16, 525–537.
Wong, M.C.S., et al., 2017. Sci. Rep. 7, 14300.
X, li, T., et al., 2012. Neoplasma 59, 622–630.
Zaporozhchenko, I.A., et al., 2018. Sci. Rep. 8, 1–13.